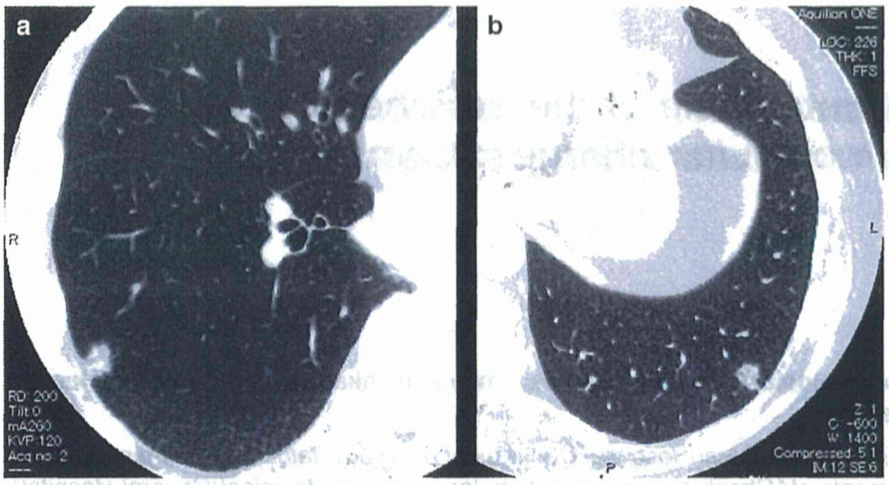

Figure 1 CT findings for (**a**) Case 1 and (**b**) Case 2. (**a**) A nodule with an irregular border measuring 12 × 10 mm was identified. Other tiny lesions were not observed in this plane. (**b**) A nodule measuring 7 × 5 mm with an irregular boarder was displayed. No other tiny lesions were present.

thoracoscopic surgery targeting the nodule was performed as a precaution. A sample obtained from the nodule was submitted for intraoperative pathological examination. The tentative diagnosis was not definitive for malignancy. The postoperative course was uneventful for approximately 7 months after the procedure.

Case 2

A 71-year-old female without complaints regularly visited the clinic for observation of a nodule in the left S9 of the lung, which had been detected at a previous check-up. She was a nonsmoker. PET-CT revealed the nodule (7 × 5 mm) had an irregular border, without accumulation, and had increased in size (Fig. 1b). The tumor markers CEA and CA19-9 were not elevated. Radiologically, the tumor did not appear to be malignant; therefore, an inflammatory lesion was suspected. On CT, minute lesions were not apparent in the background. An operation was planned to determine a definite diagnosis and curative treatment. Thoracoscopic surgery was performed, but malignancy was uncertain upon intraoperative pathological examination. The patient's postoperative course was uneventful for approximately 6 months after the procedure.

PATHOLOGICAL FINDINGS

The surgically resected specimens were fixed in 10% buffered formalin, and 5-mm thick slices were embedded in paraffin for microscopic examination. Paraffin sections were stained with hematoxylin and eosin; some paraffin sections were subjected to immunostaining using the primary antibodies listed in Table 1.

The mutational status of *EGFR* was determined by the cycleave polymerase chain reaction (PCR) method, which targeted various mutations such as G719X in exon 18, deletions involving exon 19, T790M in exon 20, L858R in exon 21, and L861Q in exon 21. *ALK* translocation was verified by fluorescent *in situ* hybridization. Formalin-fixed paraffin-embedded sections were used in both investigations.

Table 1 Antibodies used in the present study

Antibody to	Clone	Dilution	Antigen retrieval method	Source
CK7	OV-TL 12/30	Prediluted	Trypsin	Dako
CK20	Ks20.8	Prediluted	Trypsin	Dako
TTF-1	Ma695	1:100	HIER	Novocastra
CDX2	AMT28	1:50	HIER	Novocastra
MUC2	Ccp58	1:100	HIER	Novocastra
MUC5AC	CLH2	1:50	HIER	Novocastra
MUC6	CLH5	1:50	HIER	Novocastra
HNF4α	H1415	1:100	HIER	Perseus
p63	4A4	Prediluted	HIER	Nichirei
Ki-67	MIB-1	1:100	HIER	Dako
CEA	II-7	1:50	HIER	Dako

HIER, heat-induced epitope retrieval; Dako, Glostrup, Denmark; Novocastra Laboratories, Newcastle upon Tyne, UK; Perseus Proteomics, Tokyo, Japan; Nichirei Biosciences, Tokyo, Japan.

A gene mutational analysis for codons 12 and 13 of *KRAS* was performed using formalin-fixed paraffin-embedded sections and a direct sequencing method. DNA was extracted from the specimens using a QIAamp DNA FFPE Tissue Kit (Qiagen, Dusseldorf, Germany), amplified using HotStar Taq polymerase (Qiagen), and sequenced using a BigDye terminator Cycle Sequencing Kit (Applied Biosystems, Foster City, CA, USA). The first PCR was performed using primers, forward: 5′-AAAGGTACTGGTGGAGTATTTG-3′ and reverse: 5′-TGAAAATGGTCAGAGAAACC-3′. Nested PCR was performed with the primer set, forward: 5′-AACCTTATGTGT GACATGTTCTAA-3′ and reverse: 5′-GTCCTGCACCAGT AATATGC-3′. Codons 12 and 13 of *KRAS* were sequenced in

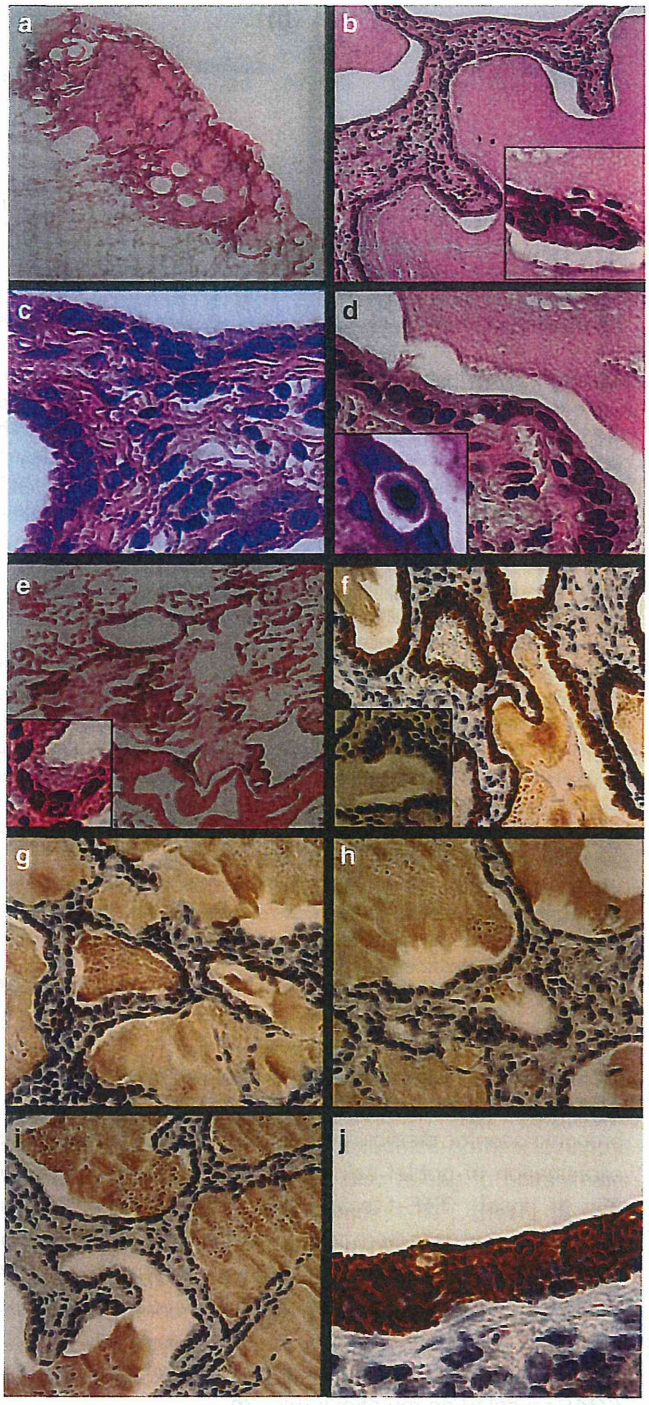

Figure 2 Histopathological and immunohistochemical findings in Case 1. (**a**) View of the entire nodule. A portion was removed for intraoperative pathological examination (×12.5). (**b**) Mucin was abundant in the air spaces of the nodule (×400). Inset, a skip lesion composed almost exclusively of goblet cells is shown (×600). (**c**) Mild nuclear atypia of overgrowing goblet cells was observed (×600). (**d**) A ciliated cell was noticeable despite this cell type being rarely encountered. (×600). Inset, a mitotic figure was detected (×1000). (**e**) A tiny focus in the pulmonary background showed a typical goblet cell metaplasia (×200). Inset, goblet cells were easily identified (×600). (**f**) Diffuse positivity for CK7 (×400). Inset, negativity for CK20 (×400). (**g**) Sparse positive cells for TTF-1 (×400). (**h**) Basal cells immunoreactive for p63 were rarely present underneath goblet cells (×400). (**i**) The Ki-67 labeling index was calculated at 4.2% (×400). (**j**) Goblet cells showed strong immunostaining for CEA (×600).

the reverse direction because sequencing in this direction provides greater accuracy judging from previous trials.

Case 1

Macroscopically, the specimen revealed a mucinous nodule, part of which was resected for intraoperative pathological examination. Postoperative microscopic examinations showed that the mucinous nodule was composed of low-height goblet cells with lepidic growth on the alveolar wall (Fig. 2a,b). Discontinuous epithelia composed almost exclusively of goblet cells, the so-called 'skip lesions,' were present at the nodule's periphery and showed lepidic growth on the alveolar septa (Fig. 2b, inset). The alveolar spaces were filled with mucin. Few ciliated cells with an eosinophilic cytoplasm were intermingled with goblet cells that showed mild nuclear atypia (Fig. 2c,d). However, scanning the entire lesion revealed a mitotic figure (Fig. 2d, inset). Basal cells underming goblet cells were sparse and hardly recognizable. Immunohistochemically, goblet cells demonstrated CK7+ (Fig. 2f), CK20– (Fig. 2f, inset), TTF-1 sparsely+ (Fig. 2g), CDX2–, and HNF4α–. Basal cells, positive for p63 were rarely detected (Fig. 2h). The Ki-67 labeling index was 4.2%, without separation by cell types (21 positive cells/500 cells; Fig. 2i). A tumor marker, CEA, showed strong immunopositivity in goblet cells (Fig. 2j). Tiny foci of goblet cell metaplasia were detected in the background with a bronchocentric distribution (Fig. 2e). Goblet cells in the tiny lesions were taller and more abundant with mucin than those in the nodule. The lesions were judged as goblet cell metaplasia of a usual type (Fig. 2e, inset). A gene analysis of the nodule showed no *EGFR* mutation or *ALK* translocation. Additional gene mutation analysis of *KRAS* revealed G12V (Fig. 3a).

Case 2

The specimen revealed a predominant nodule of a mucinous nature accompanied by minute lesions. Microscopically, the nodule contained goblet cells with abundant mucin in the cytoplasm that spilled into the alveolar spaces, and the papillary architecture was focally observed in the nodule (Fig. 4a,b). Skip lesions that mainly consisted of goblet cells were observed at the nodule's periphery (Fig. 4b, inset). Goblet cells showed slight nuclear atypia (Fig. 4c) and no mitotic figure. Basal cells were almost continuously present beneath goblet cells. Many ciliated cells with eosinophilic cytoplasm were present among goblet cells (Fig. 4d) and lined

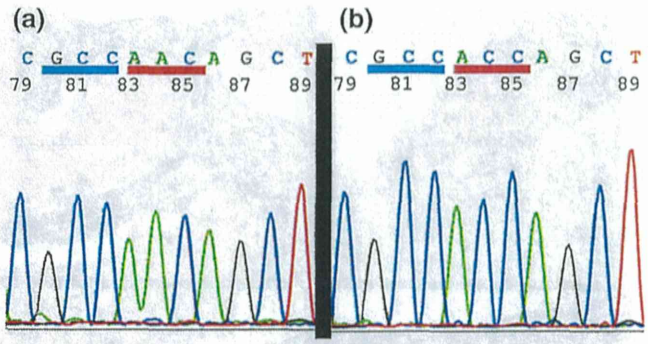

Figure 3 *KRAS* mutation analysis using the direct sequencing method. (**a**) Case 1. Codon 12 of AAC was in the reverse direction (red bar). In the forward direction, it corresponded to GTT (Val). The presence of the G12V mutation in *KRAS* was confirmed. (**b**) Case 2. Codons 12 (red bar) and 13 (blue bar) of *KRAS* were GGT and GGC, respectively, in the forward direction. No mutations were detected.

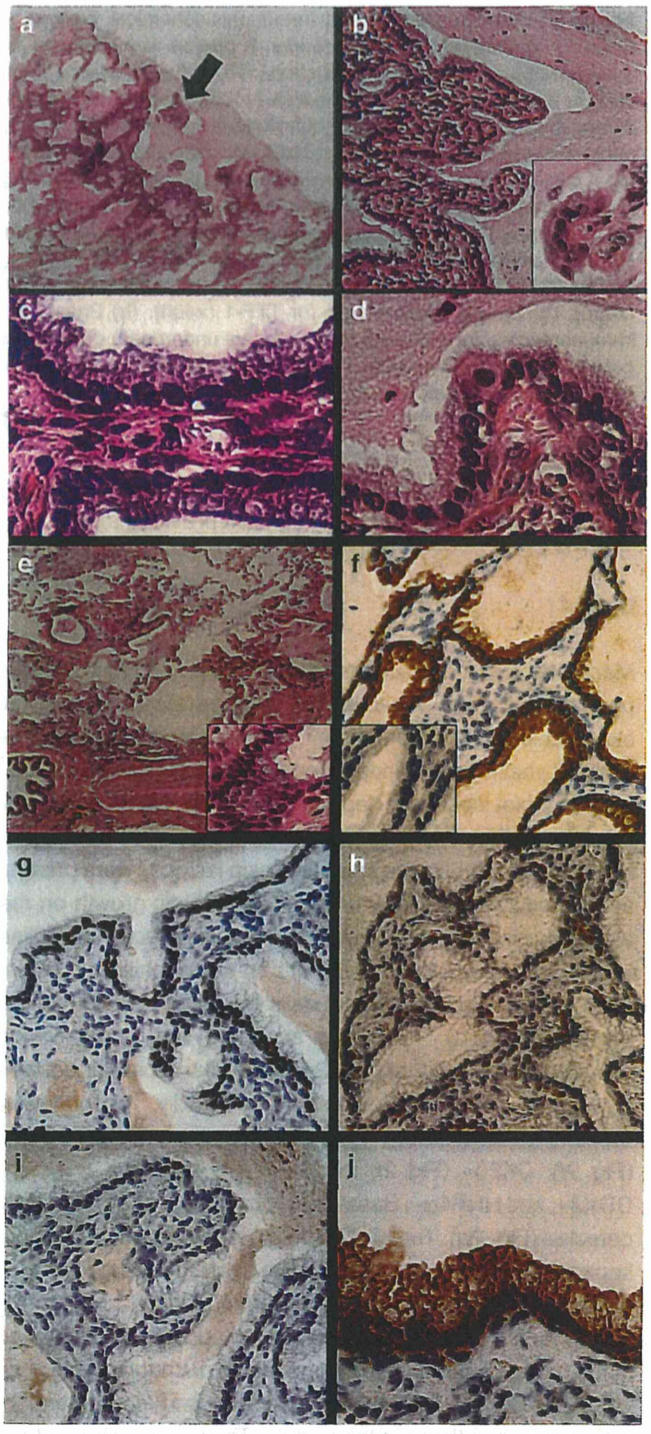

Figure 4 Histopathological and immunohistochemical findings for Case 2. (**a**) A view of the entire nodule. A part was resected for intraoperative pathological examination. A papillary architecture was observed focally (arrow) (×40). (**b**) Abundant mucin collected in the air spaces of the nodule (×400). Inset, a skip lesion that consisted mainly of goblet cells is displayed (×600). (**c**) Goblet cells showed slight nuclear atypia (×600). (**d**) Goblet cells and a conspicuous ciliated cell (×600). (**e**) A minute focus in the background of the lung showed usual goblet cell metaplasia (×200). Inset, goblet cells were easily recognized (×600). (**f**) Diffuse positivity for CK7 (×400). Inset, negativity for CK20 (×400). (**g**) Scattered cells positive for TTF-1 (×400). (**h**) Basal cells immunoreactive for p63 were almost circumferentially present beneath goblet cells (×400). (**i**) The Ki-67 labeling index was estimated at 1.8% (×400). (**j**) Goblet cells showing moderate immunostaining for CEA (×600).

the alveolar wall without invasion. Foci of typical goblet cell metaplasia were scattered in the background with a bronchiolocentric distribution (Fig. 4e). Immunohistochemical examination of goblet cells showed CK7+ (Fig. 4f), CK20– (Fig. 4f, inset), TTF-1 scatteredly+ (Fig. 4g), CDX2–, and HNF4α–. Basal cells were positive for p63 (Fig. 4h). The Ki-67 labeling index was 1.8%, including all cell types (9 positive cells/500 cells; Fig. 4i). CEA showed moderate immunopositivity in goblet cells (Fig. 4j). A gene analysis indicated no *EFGR* mutation or *ALK* translocation. An additional analysis of *KRAS* revealed no mutations (Fig. 3b).

DISCUSSION

The present cases showed multiple foci of goblet cell metaplasia that varied in size and showed a bronchiolocentric distribution. Based on previous knowledge,[1] they were believed to have resulted from long-term exposure to airway irritants such as tobacco, minerals, dust, and intrinsic and extrinsic allergens. Although peribronchiolar metaplasias are often accompanied by interstitial lung disease,[5] such as hypersensitivity pneumonitis (HP)[6] and respiratory bronchitis-associated interstitial lung disease (RB-ILD),[7] the two patients had no such disease. In Case 1, the patient had a history of smoking; a relationship between tobacco smoke exposure and an increased number of goblet cells has been documented.[8] Thus, the lesion may have resulted from smoking. In

Case 2, the patient might have been exposed to airway irritants, but no information regarding such exposure was available.

For both patients, the enlarged nodule observed on CT was clinically problematic, and their malignant potential could not be excluded. The neoplastic nature of the lesions was suspected because of the overgrowth of goblet cells, overrunning ciliated cells and basal cells, which is different from the usual goblet cell metaplasia that is often composed of more easily noticeable population of ciliated cells and basal cells.[1] A malignant lesion, such as mucinous bronchioloalveolar carcinoma (m-BAC), shares some histopathological similarities with the present cases in that goblet cells were the predominant epithelial component. Without significant variation of cytological atypia in m-BACs and our lesions, it was difficult to distinguish between them using cytological features. Based on immunohistochemistry, the varying degrees of TTF-1 attenuation in our cases mimicked m-BAC considering that TTF-1 is rarely expressed in m-BAC.[9] However, other characteristics were inconsistent with m-BAC, such as goblet cells negative for CK20[9] and the presence of p63-positive basal cells. Another difference in immunohistochemistry was negativity for P1 and P2 promoter-driven HNF4α, which is usually positive in m-BAC.[10] These immunohistochemical findings did not support a diagnosis of m-BAC in the present cases. However, the moderate to strong immunoreactivity for CEA in each case has raised the possibility that these were not merely benign lesions.

A gene mutational analysis added noticeable information in determining the nature of these lesions. As expected, *EGFR* and *ALK* were negative. However, the *KRAS* mutation of codon 12 (G12V) was an important finding in Case 1. Some data have shown the *KRAS* mutation is found especially in smoking-related lung cancers[11] and m-BAC[12,13] though the latter has no apparent relationship with smoking.[14] More recently, it was documented that a *KRAS* status could not be predicted by a smoking history alone.[15]

We speculated that the extensive goblet cell metaplasia observed in Case 1, which had a *KRAS* mutation, could be a precursor to m-BAC. Its mutation was not identified in mucous cell (goblet cell) epithelia.[16] Comparing the proliferation of goblet cells, it was found that Case 1, which had a mitotic figure, displayed a higher Ki-67 labeling index than Case 2, as expected. Moreover, there were fewer intermingled ciliated and basal cells in Case 1 than in Case 2. These findings indicated the predominant proliferation of goblet cells in Case 1. As for tumor marker CEA, the staining intensity of goblet cells was higher in Case 1 than in Case 2. The size of the lesion was also important: it was larger in Case 1 (12 × 10 mm) than in Case 2 (7 × 5 mm). These findings suggest that the lesion in Case 1 might be about to enter the malignant stage, m-BAC, and the lesion in Case 2 could be in the same neoplastic process toward m-BAC.

Recently, a newly defined tumor with a possible low-grade malignancy, ciliated muconodular papillary tumor (CMPT), has been proposed.[17–20] Ishikawa first described CMPT as a papillary tumor of the peripheral lung composed of goblet cells, ciliated columnar cells, and basal cells with abundant mucin in the air spaces.[17] Although no mutations in *KRAS*[17] and *EGFR*[20] were detected, the histopathological characteristics provoking malignancy were well documented,[17] one of which was the presence of skip lesions. Its presence in CMPT was similar to those in m-BAC. Skip lesions were present in both Cases 1 and 2. Moreover, Case 2 showed a focal papillary configuration with destruction of alveolar structures. Hence, the possibility that Case 2 was included in CMPT could not be eliminated.

In summary, we described two cases of extensive goblet cell metaplasia forming a nodule, one of which had a *KRAS* G12V mutation. These two lesions could be postulated to exist within the same category; the number of goblet cells increases as the lesion progresses to malignancy such as that observed in m-BAC. We thus consider gene mutation as a possible precancerous nature of the lesion. Considering the pulmonary background with scattered foci of usual goblet cell metaplasia, involvement of airway irritants was suspected in both cases.

ACKNOWLEDGMENTS

This work was supported in part by a Grant-in-Aid from the Ministry of Health, Labor and Welfare (21-1), National Cancer Center Research and Development Fund (26-A-8), a Grant-in-Aid from the Japan Society for the Promotion of Science (26670187), a Grant-in-Aid from the Ministry of Education, Culture, Sports, Science and Technology (221S0001), and the Smoking Research Foundation.

REFERENCES

1 Cagle PT, Roggli VL. Pathology of small airways. In: Tomashefski JF, Cagle PT, Farver CF, Fraire AE, eds. *Dail and Hammar's Pulmonary Pathology, Volume 1: Nonneoplastic Lung Disease*. New York: Springer, 2008; 886–910.
2 Reader JR, Tepper JS, Schelegle ES *et al.* Pathogenesis of mucous cell metaplasia in a murine asthma model. *Am J Pathol* 2003; **162**: 2069–78.
3 Hayashi T, Ishii A, Nakai S, Hasegawa K. Ultrastructure of goblet-cell metaplasia from Clara cell in the allergic asthmatic airway inflammation in a mouse model of asthma in vivo. *Virchows Arch* 2004; **444**: 66–73.
4 Shimizu T, Takahashi Y, Kawaguchi S, Sakakura Y. Hypertrophic and metaplastic changes of goblet cells in rat nasal epithelium induced by endotoxin. *Am J Respir Crit Care Med* 1996; **153**: 1412–8.
5 Fukuoka J, Franks TJ, Colby TV *et al.* Peribronchiolar metaplasia: A common histologic lesion in diffuse lung disease and a

rare cause of interstitial lung disease: Clinicopathologic features of 15 cases. *Am J Surg Pathol* 2005; **29**: 948–54.
6 Grunes D, Beasley MB. Hypersensitivity pneumonitis: A review and update of histologic findings. *J Clin Pathol* 2013; **66**: 888–95.
7 Yousem SA, Colby TV, Gaensler EA. Respiratory bronchiolitis-associated interstitial lung disease and its relationship to desquamative interstitial pneumonia. *Mayo Clin Proc* 1989; **64**: 1373–80.
8 Pavuluri S, Hanus V, Bergren DR. Interaction of tobacco smoke exposure and ovalbumin-sensitization promotes goblet cell and submucosal gland metaplasia in guinea pigs. *Respir Physiol Neurobiol* 2013; **189**: 639–45.
9 Rossi G, Murer B, Cavazza A *et al.* Primary mucinous (so-called colloid) carcinomas of the lung: A clinicopathologic and immunohistochemical study with special reference to CDX-2 homeobox gene and MUC2 expression. *Am J Surg Pathol* 2004; **28**: 442–52.
10 Sugano M, Nagasaka T, Sasaki E *et al.* HNF4alpha as a marker for invasive mucinous adenocarcinoma of the lung. *Am J Surg Pathol* 2013; **37**: 211–8.
11 Ahrendt SA, Decker PA, Alawi EA *et al.* Cigarette smoking is strongly associated with mutation of the K-ras gene in patients with primary adenocarcinoma of the lung. *Cancer* 2001; **92**: 1525–30.
12 Finberg KE, Sequist LV, Joshi VA *et al.* Mucinous differentiation correlates with absence of EGFR mutation and presence of KRAS mutation in lung adenocarcinomas with bronchioloalveolar features. *J Mol Diagn* 2007; **9**: 320–26.
13 Kakegawa S, Shimizu K, Sugano M *et al.* Clinicopathological features of lung adenocarcinoma with KRAS mutations. *Cancer* 2011; **117**: 4257–66.
14 Furak J, Trojan I, Szoke T *et al.* Bronchioloalveolar lung cancer: Occurrence, surgical treatment and survival. *Eur J Cardiothorac Surg* 2003; **23**: 818–23.
15 Riely GJ, Kris MG, Rosenbaum D *et al.* Frequency and distinctive spectrum of KRAS mutations in never smokers with lung adenocarcinoma. *Clin Cancer Res* 2008; **14**: 5731–4.
16 Maeshima AM, Maeshima A, Kawashima O, Nakajima T. K-ras gene point mutation in neogenetic lesions of subpleural fibrotic lesions: Either an early genetic event in lung cancer development or a non-specific genetic change during the inflammatory reparative process. *Pathol Int* 1999; **49**: 411–8.
17 Ishikawa Y. Ciliated muconodular papillary tumor of the peripheral lung: Benign or malignant? *Pathol Clin Med (Byouri-to-Rinsho)* 2002; **20**: 964–5 (in Japanese).
18 Harada T, Akiyama Y, Ogasawara H *et al.* Ciliated muconodular papillary tumor of the peripheral lung: A newly defined rare tumor. *Respir Med CME* 2008; **1**: 176–8.
19 Sato S, Koike T, Homma K, Yokoyama A. Ciliated muconodular papillary tumour of the lung: A newly defined low-grade malignant tumour. *Interact Cardiovasc Thorac Surg* 2010; **11**: 685–7.
20 Hata Y, Yuasa R, Sato F *et al.* Ciliated muconodular papillary tumor of the lung: A newly defined low-grade malignant tumor with CT findings reminiscent of adenocarcinoma. *Jpn J Clin Oncol* 2013; **43**: 205–7.

Free Radical Biology and Medicine 76 (2014) 136–146

Contents lists available at ScienceDirect

Free Radical Biology and Medicine

journal homepage: www.elsevier.com/locate/freeradbiomed

Original Contribution

Human DNA glycosylase enzyme TDG repairs thymine mispaired with exocyclic etheno-DNA adducts

Masanori Goto [a,b], Kazuya Shinmura [b,*], Yoshitaka Matsushima [c], Kousuke Ishino [a,d], Hidetaka Yamada [b], Yukari Totsuka [a], Tomonari Matsuda [e], Hitoshi Nakagama [a], Haruhiko Sugimura [b,*]

[a] Division of Cancer Development System, National Cancer Center Research Institute, 5-1-1 Tsukiji, Chuo-ku, Tokyo 104-0045, Japan
[b] Department of Tumor Pathology, Hamamatsu University School of Medicine, 1-20-1 Handayama, Higashi Ward, Hamamatsu, Shizuoka 431-3192, Japan
[c] Department of Chemistry, Hamamatsu University School of Medicine, 1-20-1 Handayama, Higashi Ward, Hamamatsu, Shizuoka 431-3192, Japan
[d] Department of Pathology, Nippon Medical School, 1-1-5 Sendagi, Bunkyo-ku, Tokyo 113-8602, Japan
[e] Research Center for Environmental Quality Management, Kyoto University, Otsu, Shiga, 520-0811, Japan

ARTICLE INFO

Article history:
Received 25 February 2014
Received in revised form
14 July 2014
Accepted 31 July 2014
Available online 20 August 2014

Keywords:
Lipid peroxidation
Etheno-DNA adducts
Base excision repair enzyme
TDG
3N^4-Ethenocytosine

ABSTRACT

Lipid peroxidation directly reacts with DNA and produces various exocyclic etheno-base DNA adducts, some of which are considered to contribute to carcinogenesis. However, the system for repairing them in humans is largely unknown. We hypothesized that etheno-DNA adducts are repaired by base excision repair initiated by DNA glycosylase. To test this hypothesis, we examined the activities of the DNA glycosylase proteins OGG1, SMUG1, TDG, NEIL1, MUTYH, NTH1, MPG, and UNG2 against double-stranded oligonucleotides containing 1,N^6-ethenoadenine (εA), 3,N^4-ethenocytosine (εC), butanone-ethenocytosine (BεC), butanone-ethenoguanine (BεG), heptanone-ethenocytosine (HεC), or heptanone-ethenoguanine (HεG) using a DNA cleavage assay. We found that TDG is capable of removing thymine that has mispaired with εC, BεC, BεG, HεC, or HεG *in vitro*. We next examined the effect of TDG against etheno-DNA adducts in human cells. TDG-knockdown cells exhibited the following characteristics: (a) higher resistance to cell death caused by the induction of etheno-DNA adducts; (b) lower repair activity for εC; and (c) a modest acceleration of mutations caused by εC, compared with the rate in control cells. All these characteristics suggest that TDG exerts a repair activity against etheno-DNA adducts in human cells. These results suggest that TDG has novel repair activities toward etheno-DNA adducts.

Introduction

Lipid peroxidation (LPO) can be generated by reactive oxygen species, nitric oxide synthases, lipoxygenases, or cyclooxygenases on polyunsaturated fatty acids (PUFAs) [1–3]. Omega-3 and omega-6 are two different kinds of PUFAs, and their peroxidation can give rise to 4-oxo-2-hexenal (4-OHE) and to 4-hydroxy-2-nonenal (4-HNE) and 4-oxo-2-nonenal (4-ONE), respectively [4–6]. These aldehydes directly react with DNA and produce exocyclic etheno-base DNA adducts, such as 1,N^6-ethenoadenine (εA), 3,N^4-ethenocytosine (εC), butanone-ethenocytosine (BεC), butanone-ethenoguanine (BεG), heptanone-ethenocytosine (HεC), and heptanone-ethenoguanine (HεG) (Supplementary Fig. S1) [1,7–10]. Recently, these etheno-DNA adducts have been detected in several human organs [11–13].

Etheno-DNA adducts are considered to lead to mutagenesis and several diseases, including cancers. For instance, vinyl chloride (VC) is known to induce εA and εC [14], and workers exposed to VC reportedly have an increased risk of the onset of hepatocellular carcinoma [15,16]. Moreover, the level of etheno-DNA adducts in patients with familial adenomatous polyposis, Crohn's disease, ulcerative colitis, or chronic pancreatitis, which predisposes an individual to cancer, is reportedly higher than that in normal tissue [17].

A few kinds of etheno-DNA adducts are reportedly removed from DNA by base excision repair (BER) initiated by DNA glycosylase. For example, εC in DNA is excised by the human DNA glycosylase enzyme TDG [18]. TDG is involved in the removal of

Abbreviations: εA, 1,N^6-ethenoadenine; εC, 3,N^4-ethenocytosine; BεC, butanone-ethenocytosine; BεG, butanone-ethenoguanine; BER, base excision repair; CAA, chloroacetaldehyde; 5-FU, 5-fluorouracil; HεC, heptanone-ethenocytosine; HεG, heptanone-ethenoguanine; HEC, 3,N^4-α-hydroxyethanocytosine; 4-HNE, 4-hydroxy-2-nonenal; LPO, lipid peroxidation; MMR, mismatch repair; 4-OHE, 4-oxo-2-hexenal; 8OHG, 8-hydroxyguanine; 4-ONE, 4-oxo-2-nonenal; PUFAs, polyunsaturated fatty acids; VC, vinyl chloride.

* Corresponding authors. Fax: +81 53 435 2225.
E-mail addresses: kzshinmu@hama-med.ac.jp (K. Shinmura), hsugimur@hama-med.ac.jp (H. Sugimura).

http://dx.doi.org/10.1016/j.freeradbiomed.2014.07.044
0891-5849/

thymine and uracil mispaired with guanine, 5-fluorouracil (5-FU) paired with G and A as well as εC from εC:G base pairs [19]. TDG is also involved in the regulation of DNA methylation through the removal of oxidized products of 5-methylcytosine, such as 5-hydroxymethyluracil, 5-formylcytosine, and 5-carboxycytosine [20–23]. εC is excised also by the DNA glycosylase enzyme SMUG1, and εA is removed by another DNA glycosylase MPG [24,25]. However, the repair mechanisms for many other LPO-related base lesions, including, in particular, 4-ONE-induced and 4-OHE-induced DNA adducts, are not fully understood. In this study, to elucidate previously unidentified repair mechanisms for etheno-DNA adducts, we examined the repair activities of eight human DNA glycosylase proteins (OGG1, SMUG1, TDG, NEIL1, MUTYH, NTH1 [also known as NTHL1], MPG, and UNG2 [also known as CCNO and a nuclear form]) against six LPO-induced DNA adducts (εA, εC, BεC, BεG, HεC, and HεG).

Material and methods

Synthesis of lipid peroxidation products and etheno-DNA adducts

Lipid peroxidation products, such as 4-OHE and 4-ONE, were respectively synthesized from the corresponding 2-alkylfurans according to previously reported methods; i.e., 2-ethylfuran (or 2-pentylfuran) was respectively oxidized by *m*-chloroperbenzoic acid in ice-cold methylene chloride to obtain 4-OHE (or 4-ONE) [26]. Successive reactions with 2′-deoxycytidine and 2′-deoxyguanosine were then respectively performed according to previously reported methods; namely 2′-deoxycytidine and about 2.8-fold molar excess amount of 4-OHE (or 4-ONE) were reacted at 60 °C in EtOH-H_2O for about 1 day, whereas in the case of the reaction of 2′-deoxyguanosine with about 3.5-fold molar excess amount of 4-OHE (or 4-ONE), the adduct formation was conducted at 37 °C in phosphate buffer (pH 7.4) and EtOH for about 4.5 days [8,9]. Ethenodeoxycytidine (εdC) was prepared by mixing with a 50% aqueous solution of chloroacetaldehyde (CAA), according to a previously reported procedure [27]. $^{15}N_5$-labeled εdC was prepared using a procedure similar to that described above for nonlabeled εdC. The more detailed synthetic procedures of the etheno-DNA adducts, including their transformations to the corresponding phosphoramidites, will be published in due course.

Plasmid construction

The *Escherichia coli* (*E. coli*) expression vectors containing human base excision repair genes were constructed by inserting the human SMUG1 and TDG cDNA sequences into a pGEX-2 T plasmid vector (GE Healthcare Bio-Science Corp., Piscataway, NJ) and the human NTH1, UNG2, and MPG cDNA sequences into a pET25b(+) plasmid vector (Novagen, Madison, WI). The *E. coli* expression vectors containing the human OGG1, NEIL1, and MUTYH cDNA sequence were used in previous papers [28–30]. All the plasmid vectors were confirmed by DNA sequencing.

Preparation of the recombinant base excision repair proteins

MUTYH and NEIL1 proteins were expressed and purified as described previously [29,30]. For the preparation of the other proteins, *E. coli* BL21-CodonPlus (DE3)-RP-competent cells (Stratagene, La Jolla, CA) were transformed with the NTH1-pET25b, UNG2-pET25b, and MPG-pET25b vectors, and *E. coli* BL21-competent cells (Stratagene) were transformed with the OGG1-pGEX-1λT, SMUG1-pGEX-2 T, and TDG-pGEX-2 T vectors. Transformed cells were cultured at 37 °C until an A_{600} of 0.6, and protein expression was induced by incubation with 0.1 mM IPTG at 15 or 20 °C. OGG1-GST, SMUG1-GST, and TDG-GST proteins were purified using glutathione Sepharose 4B (Amersham Biosciences, Piscataway, NJ) and a polyprep chromatography column (Bio-Rad, Richmond, CA), and NTH1-His_6, UNG2-His_6 and MPG-His_6 proteins were purified using TALON metal affinity resins (Clontech, Palo Alto, CA) and a TALON 2-mL disposable gravity column (Clontech). The proteins were then dialyzed against a buffer containing 10 mM sodium phosphate (pH 7.6), 50 mM NaCl, 0.5 mM DTT, 0.1 mM EDTA, 0.5 mM PMSF, 2 μg/mL pepstatin, 2 μg/mL leupeptin, 50 μM chymostatin, and 10% glycerol. The quality and concentration of each protein were determined using Image J software (National Institutes of Health, Bethesda, MD).

DNA cleavage activity assay

To prepare for the DNA cleavage activity assay, 30-mer oligonucleotides containing a single damaged base (5′-CTG GTG GCC TGA C[εA, εC, BεC, BεG, HεC or HεG]C ATT CCC CAA CTA GTG-3′) were chemically synthesized and purified using high-performance liquid chromatography (HPLC) (Bex Co., Tokyo, Japan). The oligonucleotides were ^{32}P-labeled at the 5′ terminus using a MEGA-LABEL kit (Takara, Osaka, Japan) and [γ-^{32}P]ATP (PerkinElmer, Tokyo, Japan) and then annealed to a complementary strand containing an unmodified base opposite the damaged base. Complementary oligonucleotides containing an unmodified base opposite the damaged base were also labeled at the 5′ terminus with [γ-^{32}P]ATP and then annealed to oligonucleotides containing a single damaged base. For the DNA cleavage activity assay, 300 fmol of purified OGG1, SMUG1, MPG, or NEIL1 proteins was reacted in 20 μL of a mixture containing 20 mM sodium phosphate (pH 7.6), 50 mM NaCl, 0.5 mM DTT, 0.5 mM EDTA, 1.5% glycerol, 2.5 nM labeled oligonucleotide, and 50 μg/mL BSA. Three hundred femtomoles of NTH1 or UNG2 proteins was reacted in 20 μL of a mixture containing 20 mM Hepes-KOH (pH 7.5), 50 mM NaCl, 0.5 mM DTT, 1 mM $MgCl_2$, 1.5% glycerol, 2.5 nM labeled oligonucleotide, and 50 μg/mL BSA. Three hundred femtomoles of TDG protein was reacted in 20 μL of a mixture containing 20 mM sodium phosphate (pH 7.6), 1 mM DTT, 0.5 mM EDTA, 1.5% glycerol, 2.5 nM labeled oligonucleotide, and 50 μg/mL BSA. Three hundred femtomoles of MUTYH protein was reacted in 20 μL of a mixture containing 20 mM Hepes-KOH (pH 7.5), 50 mM NaCl, 0.5 mM DTT, 0.5 mM $ZnCl_2$, 1.5% glycerol, 2.5 nM labeled oligonucleotide, and 50 μg/mL BSA. Each reaction was performed at 37 °C, and the samples were then treated with 0.1 M NaOH at 95 °C for 4 min. After the addition of denaturing formamide dye, the mixture was heated at 95 °C for 3 min and subjected to 20% PAGE. A ^{32}P-labeled marker oligonucleotide was used as a size marker for the cleavage products. The radioactivity of intact and cleaved oligonucleotides was quantified using an FLA-3000 fluoroimage analyzer (Fuji Film, Tokyo, Japan) or BAS-2500 Bio-image analyzer (Fuji Film), and ImageGauge software (Fuji Film) [31,32].

Cell survival assay

LN428-control and LN428-TDG knockdown cell lines were purchased from Trevigen (Gaithersburg, MD) and were cultured according to the manufacturer's instructions. Cells were exposed to fetal bovine serum (FBS)-free medium containing 0–700 μM CAA (Wako, Tokyo, Japan), 0–50 μM 4-ONE, or 0–50 μM 4-OHE for 2 h; the cells were then exchanged for fresh medium containing FBS. Cells were harvested 12 h after the medium change, and the percentage of cell survival was measured using a trypan blue exclusion assay.

Treatment of plasmids using an etheno-DNA adducts inducer

One hundred micrograms of pEGFP-N1 plasmids and 25 μg of the shuttle vector plasmid pMY189 containing the bacterial suppressor tRNA (*supF*) gene were treated with buffer containing 300 mM sodium cacodylate (pH 7.5) and 100 mM CAA at 37 °C for 1 h. Because the CAA-treated plasmids contained an abundance of 3,N^4-α-hydroxyethanocytosine (HEC), which is an intermediate of εC [33], after the removal of the buffer using ethanol precipitation, the CAA-treated plasmids or untreated plasmids were reacted with buffer containing 20 mM sodium cacodylate (pH 6.5) at 37 °C for 72 h to convert the HEC to εC.

To prepare plasmids containing 4-ONE-derived and 4-OHE-derived DNA adducts, 100 μg of pEGFP-N1 plasmids was treated with buffer containing 20 mM sodium phosphate (pH 7.0), 17% ethanol, and 5 mM 4-ONE at 37 °C for 3 h and with buffer containing 20 mM sodium phosphate (pH 7.0), 17% ethanol, and 20 mM 4-OHE at 37 °C for 3 h, respectively. These plasmids were purified using the Amicon Ultra Centrifugal Filter (Millipore, Bedford, MA).

Measurement of the DNA adduct level

LN428-control and LN428-TDG knockdown cells were transfected with pEGFP-N1 vector containing etheno-DNA adducts using Lipofectamine 2000 reagent (Invitrogen, Carlsbad, CA), according to the manufacturer's protocol. Cells were harvested 24 h after transfection. The plasmids were extracted using a QIAprep Spin Miniprep Kit (Qiagen, Valencia, CA). During this extraction procedure, deferoxamine was added to all the solutions at a final concentration of 0.1 mM.

The plasmids were enzymatically digested as follows: 1.6–3.2 μg pEGFP was mixed with 52 μL of digestion buffer containing 5 mM Tris-HCl (pH 7.4), 8.8 units of DNase I (Wako), and internal standards. After incubating at 37 °C for 3 h, 2 μL of 300 mM sodium acetate (pH 5.3), 2 μL of 1 M $ZnCl_2$, and 3 μL of 1.6 units/μL nuclease P1 (Wako) were added and the mixtures were incubated for a further 3 h at 37 °C. After this incubation, 2 μL of 500 mM Tris base and 140 units/μL of alkaline phosphatase (Wako) and 20 units/μL of phosphodiesterase I (Wako) were added and the mixture was incubated for 18 h at 37 °C. Because the mass of εdC is consistent with that of deoxyadenosine and their peaks overlap [34], to convert adenosine to inosine, which has a different mass, 0.5 μL of adenosine deaminase (Sigma, St. Louis, MO) was added to the reaction solution and the sample was incubated for 1 h at 25 °C. The sample was then purified using Sep-pak C18 cartridges (Water, Milford, MA) and collected as 20% methanol fractions. The fractions were evaporated to dryness and then resuspended in 66.7 μL of distilled water. Fifteen microliters of the eluate was subjected to liquid chromatography coupled with tandem mass spectrometry (LC-MS/MS). The DNA adducts were quantified using LC-MS/MS, as described previously [35], and positive ions were acquired in multiple reaction monitoring (MRM) mode. The MRM transitions were monitored using the following cone voltages and collision energies: εdC [252.1→136.05, 35 V, 14 eV], $^{15}N_3$-εdC [255.1→139.05, 35 V, 14 eV], heptanone-ethenodeoxycytidine (HεdC) [364.2→248.15, 35 V, 14 eV], $^{15}N_3$-HεdC [367.2→251.15, 35 V, 14 eV], butanone-ethenodeoxycytidine (BεdC) [322.13→206.08, 35 V, 14 eV], $^{15}N_3$-BεdC [325.13→209.08, 35 V, 14 eV], butanone-ethenodeoxyguanisine (BεdG) [362.13→246.08, 35 V, 14 eV], and $^{15}N_5$-BεdG [367.13→251.08, 35 V, 14 eV]. Quantification was performed from standard curves constructed using the ratio of known amounts of authentic standards and internal standards. The adduct levels were normalized to the amounts of DNA.

SupF forward mutation assay

LN428-control and LN428-TDG knockdown cells were trypsinized and washed in PBS(−); the cells were then suspended in Gene Pulser electroporation buffer (Bio-Rad). A total of 5×10^6 cells plus 5 μg of shuttle plasmids was placed in a Gene Pulser Cuvette for a 0.4-cm electrode (Bio-Rad), and electroporation was performed using a Gene Pulser II apparatus (Bio-Rad) at 220 V and 950 μF. The cells were incubated at 37 °C for 72 h. The propagated plasmids were then extracted from the cells and digested with *Dpn*I to eliminate unreplicated plasmids. The plasmids were introduced into the KS40/pKY241 indicator *E. coli* strain using electroporation. The transformants were plated onto LB agar plates containing nalidixic acid, ampicillin, chloramphenicol, IPTG, and X-gal. White colonies on this plate were counted as *supF* mutants. The mutation frequencies were calculated as the number of *supF* mutants per the total number of transformants, which were counted on LB plates containing ampicillin, chloramphenicol, IPTG, and X-gal. The mutations in the *supF* gene were then analyzed as described previously [36].

Results

DNA glycosylase activity against oligonucleotide containing etheno-DNA adducts

To investigate the repair mechanism of the LPO-induced DNA adducts εA, εC, BεC, BεG, HεC, and HεG, we first prepared eight purified recombinant DNA glycosylase proteins: OGG1, SMUG1, TDG, NEIL1, MUTYH, NTH1, MPG, and UNG2 (Supplementary Fig. S2A). To confirm that the DNA glycosylase proteins prepared using our system actually possessed enzymatic activity, we examined the repair activity of each protein toward an oligonucleotide containing a previously known substrate using a DNA cleavage assay [25,28–31,37,38]. The oligonucleotides that reacted with DNA glycosylase protein were analyzed on a denaturing polyacrylamide gel and their mobility was compared with that of a marker oligonucleotide. Substantial repair activity was shown for all the proteins (Supplementary Fig. S2B). Next, we prepared double-stranded oligonucleotides containing εA, εC, BεC, BεG, HεC, or HεG paired with unmodified A, C, G, or T. For each double-stranded oligonucleotide, [γ-^{32}P]ATP labeling at the 5′ terminus was performed for etheno-adduct-containing oligonucleotides or unmodified oligonucleotides, meaning that we can evaluate DNA glycosylase activity toward the etheno-DNA adduct itself and an unmodified base paired with an etheno adduct. When an oligonucleotide containing an εA adduct was reacted with the DNA glycosylases, the cleavage product was detected in the lanes of the reaction of the MPG protein and an oligonucleotide containing εA:A, εA:T, εA:C, or εA:G, which agreed with previous findings [37] (Fig. 1A). When an oligonucleotide containing an εC adduct was reacted, the cleavage product was detected in the lanes of the reaction of the SMUG1 protein and an oligonucleotide containing εC:A, εC:T, εC:C, or εC:G and in the lane of the reaction of the TDG protein and an oligonucleotide containing εC:G (Fig. 1B). Although the cleavage activity of SMUG1 and TDG to the εC:G substrate has been previously reported [24,25], the effects of SMUG1 on the εC:A, εC:T, and εC:C substrates are novel findings. Since the DNA cleavage assay against εC and HεC showed signal background at the cleavage product position to some extent, there was some difficulty in judging the cleavage activity of some proteins (Figs. 1B and 3A). So, we extended a reaction time to 1 h, and examined DNA glycosylase activity toward an oligonucleotide containing εC and HεC again (Supplementary Fig. S3). The background was still detected not only in the lanes of oligonucleotides reacted with DNA glycosylases but also in the lane of an oligonucleotide treated only with alkali. The background levels in the lanes of the reaction of OGG1, NTH1, UNG2, MPG, MUTYH, or NEIL1 with εC-containing oligonucleotide and those in the lanes of the reaction of the all the

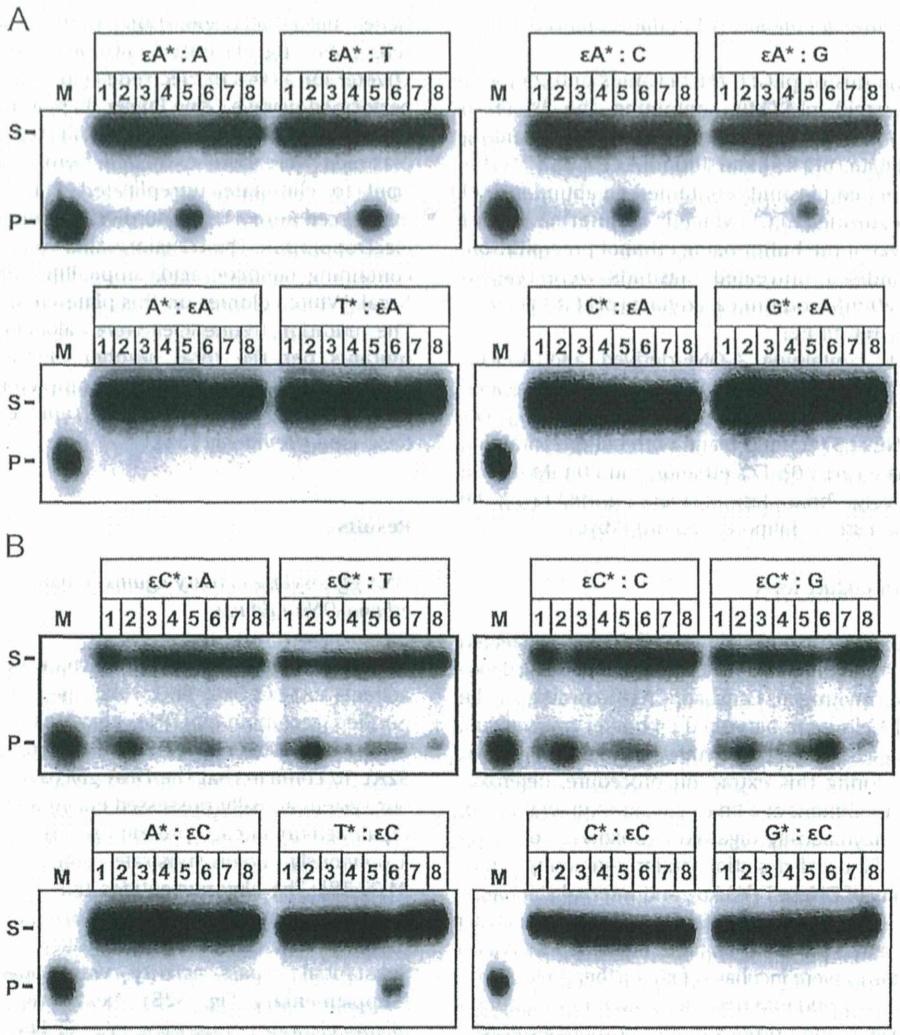

Fig. 1. Evaluation of repair activities of 8 DNA glycosylase proteins against 1,N^6-ethenoadenine (εA) and 3,N^4-ethenocytosine (εC). The abilities of the DNA glycosylase proteins OGG1, SMUG1, NTH1, UNG2, MPG, TDG, MUTYH, and NEIL1 to repair double-stranded DNA containing εA (A) or εC (B) were examined using a DNA cleavage assay. Each BER protein (300 fmol) was allowed to act on a double-stranded oligonucleotide containing εA or εC at 37 °C for 30 min. The asterisks show the 5′-labeled ^{32}P-labeled oligonucleotides, consisting of εA-containing and εC-containing oligonucleotides in the upper panels of (A) and (B), respectively, and unmodified oligonucleotides in the lower panels of (A) and (B). Numbers 1, 2, 3, 4, 5, 6, 7, and 8 indicate OGG1, SMUG1, NTH1, UNG2, MPG, TDG, MUTYH, and NEIL1, respectively. A ^{32}P-labeled marker oligonucleotide was used as a size marker for the cleavage products. The intact 30-mer oligonucleotides (substrate) and cleavage products are indicated by S and P, respectively. The reference numbers for OGG1, SMUG1, NTH1, UNG2, MPG, TDG, MUTYH, and NEIL1 proteins are NP_002533.1, NP_001230716.1, NP_002519.1, NP_550433.1, NP_002425.2, NP_003202.3, NP_001041639.1, and NP_078884.2, respectively.

DNA glycosylases with HεC-containing oligonucleotide were nearly identical to the signal seen in the lane of εC- or HεC-containing oligonucleotide treated only with alkali. These results mean that OGG1, NTH1, UNG2, MPG, MUTYH, and NEIL1 do not have the activity against εC, and all eight DNA glycosylase proteins do not have activity against HεC. Furthermore, cleavage product was also detected in the lane of the reaction of the TDG protein and the oligonucleotide containing an unmodified T mispaired with εC (Fig. 1B). Interestingly, and most unambiguously, when an oligonucleotide containing a BεC, BεG, HεC, or HεG adduct was reacted, the TDG protein also showed cleavage activity against unmodified T mispaired with BεC, BεG, HεC, or HεG (Figs. 2 and 3). These TDG activities toward unmodified T mispaired with etheno adducts have not been reported, meaning that they are novel findings. Next, to further investigate the cleavage activity of TDG, TDG protein was reacted with substrate for various time periods (i.e., a time-course assay) and the percentage of cleaved products per total oligonucleotide was calculated and expressed as the percentage incision. The time-course assay clearly demonstrated that the εC glycosylase activity of TDG against oligonucleotides containing an εC:G base pair and the unmodified T cleavage activity of TDG against the oligonucleotides containing T:εC, T:BεC, T:BεG, T:HεC, or T:HεG mispairs increased in a time-dependent manner (Fig. 4). Meanwhile, no clear cleavage products were detected when an oligonucleotide containing an unmodified C:G and T:A base pairs was reacted with the TDG protein. Interestingly, the level of cleavage activity of TDG against T is strongly influenced by the kind of opposite etheno adduct. These results suggested that TDG is capable of excising T paired with εC, BεC, BεG, HεC, or HεG as well as εC in the εC:G pair.

Role of TDG on cell death caused by inducers of etheno-DNA adducts in human cells

CAA, which is a VC metabolite, induces etheno adducts (including εC) into genomic DNA, similar to VC [39]. To investigate whether the TDG protein has any effect on the viability of cells exposed to an etheno-DNA adduct inducer, an LN428-TDG-knockdown cell line and its control cell line were treated with CAA, 4-ONE, or 4-OHE for 2 h; after 12 h, cell survival was measured. A higher survival was shown in TDG-knockdown cells than in control cells when exposed to 450–700 μM CAA (Fig. 5A).

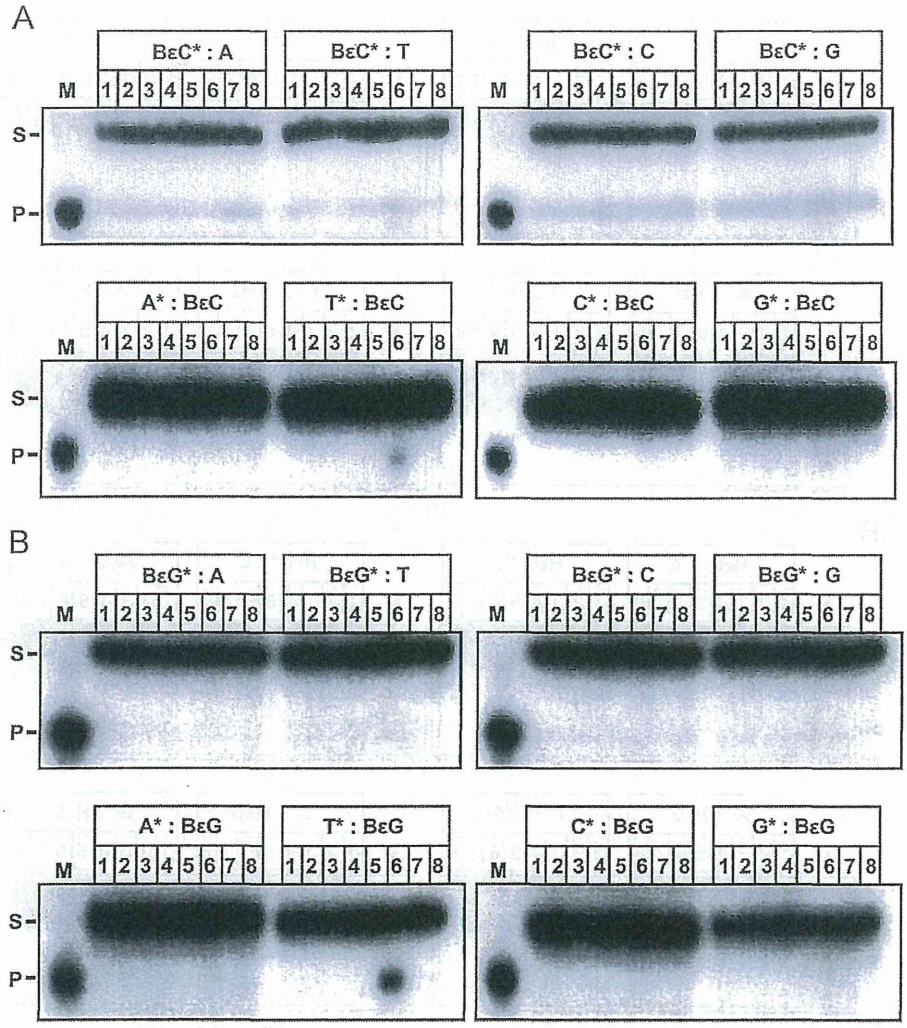

Fig. 2. Evaluation of repair activities of 8 DNA glycosylase proteins against 4-oxo-hexenal adducts. The abilities of the DNA glycosylase proteins OGG1, SMUG1, NTH1, UNG2, MPG, TDG, MUTYH, and NEIL1 to repair double-stranded DNA containing butanone-ethenocytosine (BεC) (A) or butanone-ethenoguanine (BεG) (B) were examined using a DNA cleavage assay. Each BER protein (300 fmol) was allowed to act on a double-stranded oligonucleotide containing BεC or BεG at 37 °C for 30 min. The asterisks show the 5′-labeled ^{32}P-labeled oligonucleotides, consisting of BεC-containing and BεG-containing oligonucleotides in the upper panels of (A) and (B), respectively, and unmodified oligonucleotides in the lower panels of (A) and (B). Numbers 1, 2, 3, 4, 5, 6, 7, and 8 indicate OGG1, SMUG1, NTH1, UNG2, MPG, TDG, MUTYH, and NEIL1, respectively. A ^{32}P-labeled marker oligonucleotide was used as a size marker for the cleavage products. The intact 30-mer oligonucleotides (substrate) and cleavage products are indicated by S and P, respectively.

The survival of cells exposed to 5–30 μM 4-ONE or 4-OHE tended to decrease similarly in both control cells and TDG knockdown cells, whereas the cell survival of TDG-knockdown cells was significantly higher than that of control cells when treated with 50 μM 4-ONE or 4-OHE (Fig. 5B and C). These data suggested that TDG promotes cell death induced by etheno-DNA adducts.

Activity of TDG for the repair of etheno-DNA adducts in human cells

To determine whether TDG is capable of repairing etheno-DNA adducts in human cells, we attempted to investigate the ability of TDG to suppress etheno-DNA adduct levels in human cells. First, we treated pEGFP-N1 plasmid with CAA, 4-ONE, or 4-OHE and measured the levels of εdC, HεdC or butanone-etheno adducts, respectively, using an LC-MS/MS analysis. A dramatic increase was observed in the levels of εdC, HεdC, and butanone-etheno adducts (Supplementary Fig. S4). TDG-knockdown cells and control cells were then transfected with plasmids treated using CAA, 4-ONE, or 4-OHE; after 24 h, the plasmids were collected and their adduct levels were measured using an LC-MS/MS analysis. The adduct levels of εdC, HεdC, BεdC, and BεdG were significantly reduced in both the TDG-knockdown cells and the control cells (Fig. 6), indicating the repair of these adducts in human cells. No significant differences in the levels of HεdC, BεdC and BεdG were seen between the TDG-knockdown cells and the control cells (Fig. 6B–D); however, remarkably, the εdC level of plasmids collected from the TDG-knockdown cells was significantly higher than that of plasmids collected from the control cells (Fig. 6A). This result suggests that TDG has the capacity to remove εC in human cells.

Effect of TDG on mutation spectrum of etheno-DNA adducts in human cells

Next, to study the functional characteristics of TDG against mutations caused by etheno-DNA, we prepared a shuttle plasmid pMY189 treated or not treated with 100 mM CAA; the mutation frequency was then compared between the TDG-knockdown cells and their control cells using a *supF* forward mutation assay and both kinds of plasmids. The mutation frequency in the *supF* of CAA-treated pMY189 was significantly higher than that of non-treated pMY189 in both the control and the TDG-knockdown cells (Figs. 7A, $P < 0.05$). When the mutation frequency in CAA-treated pMY189 was compared between the control and the TDG-knockdown cells, the mutation frequency in the TDG-knockdown